Auroral electrojets variations caused by recurrent high-speed solar wind streams during the extreme solar minimum of 2008

Jianpeng Guo,[1] Xueshang Feng,[1] T. I. Pulkkinen,[2] E. I. Tanskanen,[3,4] Wenyao Xu,[5] Jiuhou Lei,[6] and Barbara A. Emery[7]

Received 17 December 2011; revised 10 February 2012; accepted 16 February 2012; published 6 April 2012.

[1] The IMAGE network magnetic measurements are used to investigate the response of the auroral electrojets to the recurrent high-speed solar wind streams (HSSs) during the extreme solar minimum period of 2008. We first compare the global AU/AL indices with the corresponding IU/IL indices determined from the IMAGE magnetometer chain and find that the local IMAGE chain can better monitor the activity in MLT sectors 1230–2230 for IU and 2230–0630 for IL during 2008. In the optimal MLT sectors, the eastward and westward electrojets and their central latitude reveal clear 9-day periodic variations associated with the recurrent HSSs. For the 9-day perturbations, both the eastward and westward electrojet currents are better correlated with parallel electric field (E_{PAR}) and electron hemispheric power (HPe) than with other forcing parameters. Interestingly, the eastward electrojet shows good correlations ($r > 0.6$) with E_{PAR} and HPe only in part of its optimal MLT-sector, roughly 1200–1800, while the westward electrojet shows good correlations ($r < -0.6$) with E_{PAR} and HPe in its whole optimal MLT sector. The poor correlations between the eastward electrojet and E_{PAR} and HPe in the MLT sector 1800–2200 might be attributed to the impact of other magnetosphere-ionosphere coupling processes. The sensitivities of the eastward and westward electrojet currents to E_{PAR} are close to 0.06 MA/(mV/m) and −0.12 MA/(mV/m), respectively, and the sensitivities of their central latitudes to E_{PAR} are close to −2.83 Deg/(mV/m) and −2.14 Deg/(mV/m), respectively. The observed auroral electrojet response to the recurrent solar wind forcing provides new opportunities to study the physical processes governing the eastward and westward auroral electrojets.

Citation: Guo, J., X. Feng, T. I. Pulkkinen, E. I. Tanskanen, W. Xu, J. Lei, and B. A. Emery (2012), Auroral electrojets variations caused by recurrent high-speed solar wind streams during the extreme solar minimum of 2008, *J. Geophys. Res.*, *117*, A04307, doi:10.1029/2011JA017458.

1. Introduction

[2] During the extremely low solar activity period of 2008 when solar EUV flux is low and nearly constant, strong and long solar wind high-speed streams (HSSs) emanating from near-equatorial coronal holes are typical and dominate the solar-terrestrial connection [*Gibson et al.*, 2009]. HSSs recur with harmonic solar rotational periodicities at 13.5 and 9 days [*Tulasi Ram et al.*, 2010]. *Lei et al.* [2011] suggested that the harmonic periodicities are linked to the spatial distribution of long-lived, low to middle latitude coronal holes. As the streams travel in interplanetary space, they catch up with the preceding slow-speed streams and create the corotating interaction regions (CIRs) at the interfaces between the two streams [*Tsurutani et al.*, 1995]. On arrival at the Earth's magnetopause, such streams and CIRs modulate energy transfer into the magnetosphere-ionosphere-thermosphere system and trigger recurrent geomagnetic disturbances [e.g., *Tanskanen et al.*, 2005]. In response to the high-latitude energy injection, the ionospheric and thermospheric properties such as electron density and thermospheric density are also found to oscillate with the same periodicities [e.g., *Tulasi Ram et al.*, 2010; *Lei et al.*, 2011]. Since high-latitude energy deposition is also known to drive auroral eletrojets, we will investigate whether the periodic variations noted in the solar wind produce a detectable signature in the auroral electrojet activity. It is important to note that, however, the high-latitude energy injection is actually

[1]SIGMA Weather Group, State Key Laboratory of Space Weather, Center for Space Science and Applied Research, Chinese Academy of Sciences, Beijing, China.
[2]School of Electrical Engineering, Aalto University, Aalto, Finland.
[3]Finnish Meteorological Institute, Helsinki, Finland.
[4]Department of Physics and Technology, University of Bergen, Bergen, Norway.
[5]Institute of Geology and Geophysics, Chinese Academy of Sciences, Beijing, China.
[6]School of Earth and Space Sciences, University of Science and Technology of China, Hefei, China.
[7]High Altitude Observatory, National Center for Atmospheric Research, Boulder, Colorado, USA.

0148-0227/12/2011JA017458

controlled by two main energy transfer processes: solar wind-magnetopause interaction processes (directly driven processes) and energy release processes in the magnetotail (loading-unloading processes). When energy and particles are transferred from the solar wind to the magnetosphere via dayside reconnection, usually both the eastward and westward auroral electrojets experience a smooth enhancement. Meanwhile, a part of the solar-wind energy and particles is stored into the magnetotail. When magnetospheric activity exhibits strong bursts such as substorms, the energy and particles stored in the magnetotail may dissipate abruptly to the high-latitude ionosphere, causing an extra strong westward electrojet to the midnight sector [*Kauristie et al.*, 1996; *Kallio et al.*, 2000].

[3] The primary objective of this paper is to investigate the response of the auroral electrojets to the recurrent high-speed solar wind streams (HSSs) during 2008 using the IMAGE network magnetic measurements. In this context, first, we compare the global AU/AL indices with the corresponding IU/IL indices determined from the IMAGE magnetometer chain and find out the IMAGE optimal coverage period during solar minimum. Second, we focus our investigation mainly on the 9-day periodicity in the auroral electrojet activity associated with the recurrent HSSs. Further, we discuss the observed results as well as some additional and important implications.

2. Data Sets

[4] The primary data source used in this work is the geomagnetic field at 10 s cadence recorded by the IMAGE magnetometer stations. The IMAGE magnetometer chain consists of 31 magnetometers ranging in latitude from 58° (Tartu, Estonia) to 79° (Ny-Ålesund, Svalbard), or from 54° to 75° in corrected geomagnetic coordinates [*Tanskanen*, 2009]. The stations have longitudinal coverage over about 30° from western Norway to the Kola peninsula. The locations of the IMAGE magnetometer stations are shown in Figure 2 of *Pulkkinen et al.* [2011]. The data are processed in a way analogous to the AU/AL indices to produce the IU/IL indices [*Tanskanen et al.*, 2002]. While the indices can be computed for all local times, the IL index gives a better estimate than the AL index for the global activity in the local time sector 2230–0630 MLT (described in section 3). Similarly, the eastward electrojet response to the IU index is clearly visible only in the local time sector 1230–2230 MLT. From the longitudinal chain, we process the properties of the eastward and westward electrojets, in particular the equivalent maximum current density and total current as well as the latitude of the maximum current density [*Amm and Viljanen*, 1999; *Pulkkinen et al.*, 2003].

[5] In addition, the solar wind magnetic field and plasma parameters are available from the 1-h averaged OMNI database (GSM coordinates at 1 AU). Global auroral precipitation estimates on a 1 h cadence are computed by using data from Defense Meteorological Satellite Program (DMSP) and National Oceanic and Atmospheric Administration (NOAA) satellites intercalibrated with each other by *Emery et al.* [2008; 2009]. For the present study, we use the hourly estimates of the electron hemispheric power (HPe) and the ion hemispheric power (HPi) from the Northern Hemisphere and confine ourselves to auroral energies <20 keV.

3. IMAGE Optimal Coverage Period

[6] *Pulkkinen et al.* [2011] investigated the auroral electrojet activity during deep solar minimum at the end of solar cycle 23 using data from the IMAGE magnetometer chain and found that the electrojets moved to more poleward latitudes during 2008–2009 than during other times. In order to find out the IMAGE optimal coverage period during 2008, we use the same method as *Kauristie et al.* [1996] and compare the global AU/AL indices with the corresponding IU/IL indices by computing the average relative error, E(t), which is defined, e.g., for AL, as

$$E_{AL}(t) = \frac{AL(t) - IL(t)}{AL(t)} \tag{1}$$

where t is the time (with 1-min resolution). AL and IL are negative and thus E_{AL} is negative when the local IMAGE chain sees stronger activity than the global one (i.e., when $IL < AL$, but ($|IL| > |AL|$). In this case the deviation is due to the improvement in the local index when compared to the global one. When the local IMAGE chain is outside the key region, $|IL| \sim 0$ and $E_{AL} \sim 1$. These limit values are valid also for E_{AU} when defined similarly as E_{AL}. The relative errors are then binned to 1-h UT bins. The 1-h averages are used for defining the optimal UT periods when the relative errors are below 0, which we consider as a more reasonable level for global activity monitoring. Our definition for the relative error does not take into account the periods when $AL > 0$ or $AU < 0$. Such periods, however, are rare and thus not statistically significant. The UT dependence of the relative errors E_{AU} and E_{AL} are shown in Figure 1. The average relative errors are below 0 during ~1000–2000 UT (1230–2230 MLT) and ~2000–0400 UT (2230–0630 MLT) for IU and IL, respectively. That is, in MLT sectors 1230–2230 (for IU) and 2230–0630 (for IL), the IMAGE magnetometer chain gives a better estimate for the global activity during 2008. The explanation is that the poleward shift of the electrojet during solar minimum causes the standard observatories (global AU/AL indices) to escape from the zone directly influenced by the electrojets. Nevertheless, the IMAGE chain can give more information of the real situation but, of course, only during some limited UT period.

[7] Then the electrojet data from the optimal MLT sectors can be used to investigate the responses of the auroral electrojets to the recurrent HSSs. For the eastward electrojet, we compute the hourly averages of the total current (EEJ) and the central latitude (Lat-EEJ) in the MLT sector 1200–2200. For the westward electrojet, we compute the hourly averages of the total current (WEJ) and the central latitude (Lat-WEJ) in the MLT sector 2200–0600. Note that for computing the 1-h averages we actually use the data from the MLT periods which are half an hour before the optimal MLT sectors. In spite of large variability (not shown), distinct variation patterns are visible in the hourly averages. To reveal these patterns, the daily averages of the total currents (EEJ and WEJ) and their central latitudes (Lat-EEJ and Lat-WEJ) are shown in Figure 2. Note that the current direction is defined such that the westward current is negative, and it is plotted in

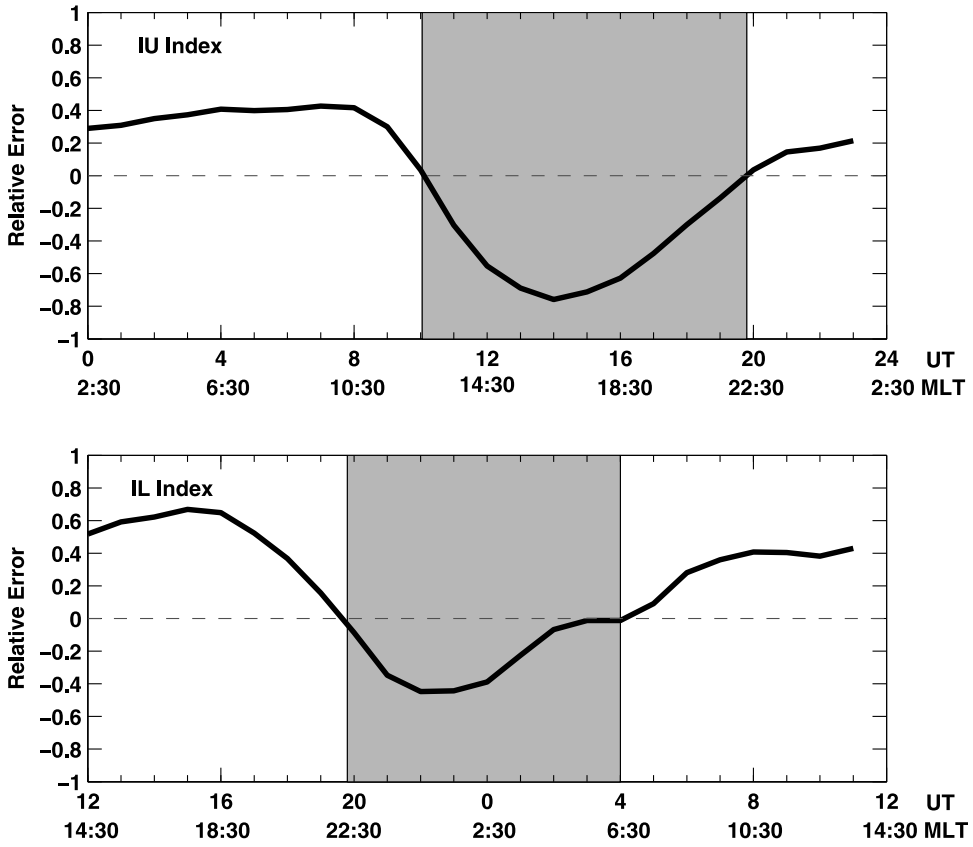

Figure 1. Universal time (UT) dependence of the average relative errors between (top) AU and IU and (bottom) AL and IL during the extreme solar minimum year 2008. The UT periods when the error is below 0 (i.e., the local IMAGE chain sees stronger activity than the global one) are shaded.

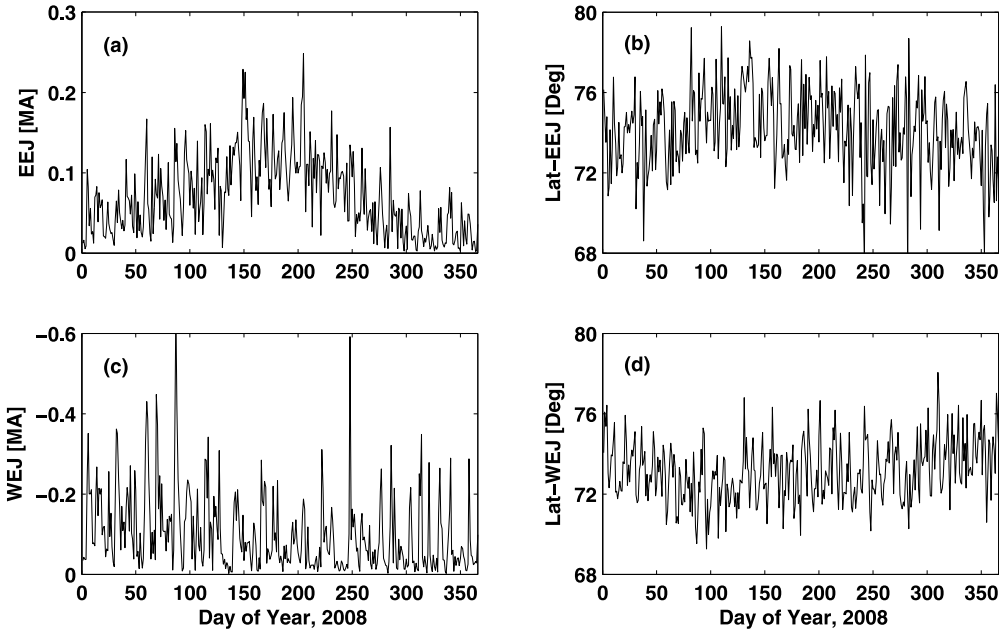

Figure 2. Daily mean variations in the total (a) eastward and (c) westward electrojet currents (EEJ and WEJ) and (b and d) their central geographic latitudes (Lat-EEJ and Lat-WEJ) during 2008. Note that the eastward and westward electrojet currents are positive and negative, respectively, and the westward electrojet is plotted in reversed scale such that the magnitude of the current increases upward.

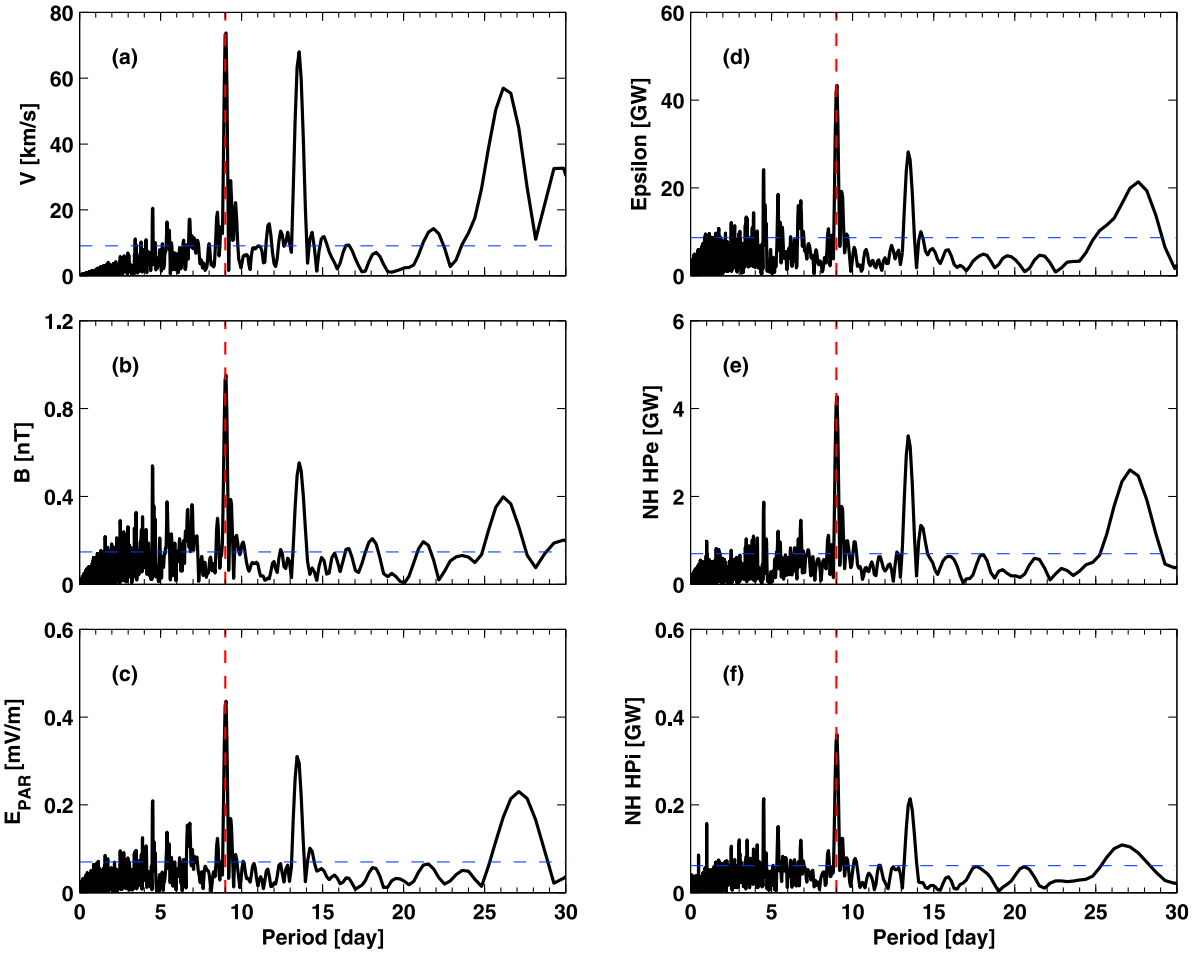

Figure 3. Lomb-Scargle spectral amplitudes of (a) solar wind velocity V, (b) interplanetary magnetic field B, (c) parallel electric field E_{PAR} [*Pulkkinen et al.*, 2010], (d) solar wind energy input (the epsilon parameter) [*Akasofu*, 1981], (e) Northern Hemisphere (NH) electron hemispheric power (HPe), and (f) NH ion hemispheric power (HPi) during the extreme solar minimum year 2008. The horizontal dashed lines represent the 99% significance level, and the vertical dashed lines denote the period at 9 days.

a reversed scale with the absolute value of the current intensity increasing upward. Clearly, both EEJ and WEJ present high-frequency peaks (within each solar rotation period), which are imbedded in the larger timescale variations due to the seasonal variation [see *Pulkkinen et al.*, 2011].

4. Auroral Electrojets Oscillations Due to Periodic Solar Wind Forcing

[8] Lomb-Scargle periodograms [*Lomb*, 1976; *Scargle*, 1982] are calculated on solar wind velocity V, interplanetary magnetic field B, parallel electric field E_{PAR}, solar wind energy input (the epsilon parameter), Northern Hemisphere (NH) electron hemispheric power (HPe), and NH ion hemispheric power (HPi) to determine the periodicities during 2008. The corresponding results are shown in Figure 3. The horizontal dashed lines represent the 99% significance level. The parallel electric field is defined as $E_{PAR} = E \sin(\theta/2)$, where E is the magnitude of the solar wind electric field computed as $-V \times B$ and θ is the interplanetary magnetic field (IMF) clock angle. The component E_{PAR} gives the electric field component roughly along the large-scale neutral line at the magnetopause and thus is a measure of the reconnection efficiency at the dayside magnetopause [*Pulkkinen et al.*, 2010]. The epsilon parameter is defined as $\varepsilon = (4\pi/\mu_0)vB^2 \sin^4(\theta/2)l_0^2$, where θ is the IMF clock angle and $l_0 = 7R_E$ is an empirical scaling parameter [*Akasofu*, 1981]. Figures 3a–3b clearly show that solar wind parameters (V and IMF B) exhibit pronounced spectral peaks at the periods of 27, 13.5, and 9 days above the 99% significance level. Both solar wind velocity and IMF B affect the magnetic reconnection rate in the magnetosphere, such as E_{PAR}, which do exhibit the corresponding spectral peaks (Figure 3c). As the dayside merging rate determines the rate of solar wind energy and particle entry into the magnetosphere, it is expected that the solar wind energy input and the auroral hemispheric power (HP) will change coherently with the merging rate. Indeed, Figure 3d (the epsilon parameter) and Figures 3e–3f (HPe and HPi) provide such evidence, respectively. Further, the corresponding periodic oscillations in auroral electrojet activity would be expected. Recall from the electrojet data that the oscillations with multiday periods are clearly seen in both the eastward

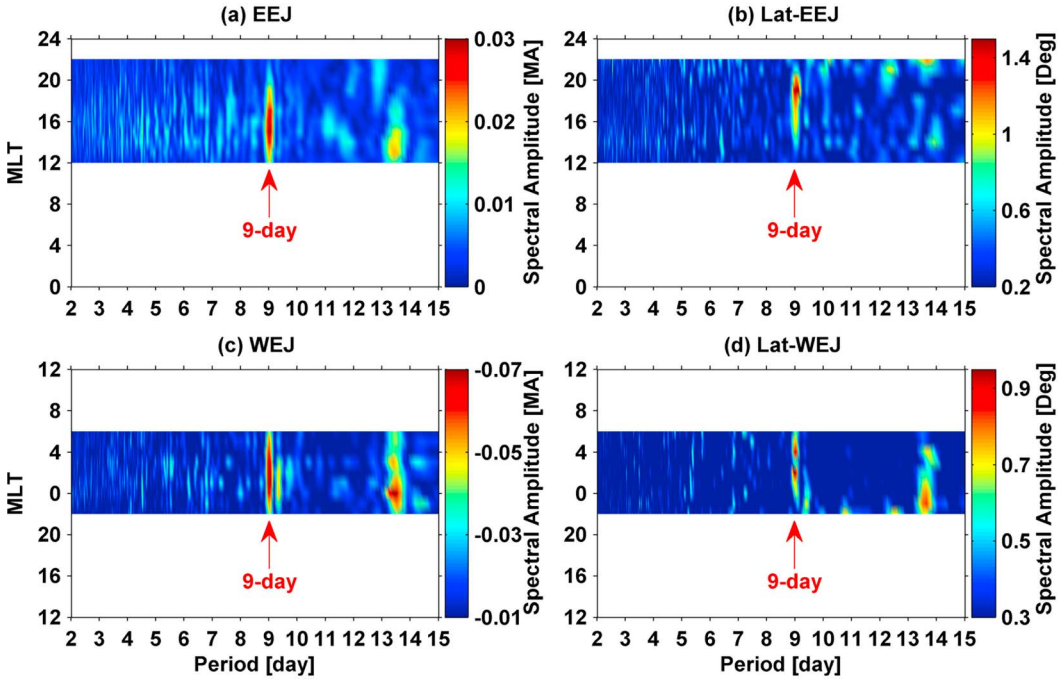

Figure 4. Contour plots of spectral amplitudes of the total (a) eastward and (c) westward electrojet currents (EEJ and WEJ) in MA and (b and d) their central geographic latitudes (Lat-EEJ and Lat-WEJ) in degrees as a function of MLT (only the optimal MLT sectors) and periods in 2008. The red arrows mark the period at 9 days.

and westward electrojet currents (cf. Figure 2). However, it is important to note that, although the 27-day and 13.5-day periodicities are present in solar wind parameters and also particle precipitation, they may not be solely responsible for recurrent auroral electrojet activity because 27-day and 13.5-day periodicities also exist in solar EUV irradiance which directly impacts the ionospheric Hall conductance [*Ahn et al.*, 1999]. Therefore we will mainly focus on confirming if the 9-day periodicity exists in auroral electrojet activity and varies in the same manner as solar wind parameters as well as particle precipitation.

[9] To examine the 9-day periodicity in the auroral electrojet parameters: the total eastward and westward electrojet currents (EEJ and WEJ), and their central latitudes (Lat-EEJ and Lat-WEJ), Lomb-Scargle analysis is performed in each MLT bin. The periodograms are shown in Figures 4a–4d for EEJ, Lat-EEJ, WEJ, and Lat-WEJ, respectively. The strong 9-day periodicity is evident in these auroral electrojet parameters. Moreover, the spectral amplitudes of the 9-day periodicity vary with MLT. The coexistence of the 9-day periodic variation in both the solar wind parameters and the auroral electrojet parameters supports the cause and effect relationship between HSSs and auroral electrojet activity.

[10] In order to examine the relationship between the 9-day periodicities in the auroral electrojet and particle precipitation as well as solar wind parameters, we apply a band-pass filter to each MLT bin of the electrojet parameters. The band-pass filter is centered at 9 days, with half-power points at 6 and 12 days. Figures 5a–5d show the MLT variations of band-pass filtered 9-day perturbations in the electrojet parameters such as EEJ, Lat-EEJ, WEJ, and Lat-WEJ. The superimposed black curve in each plot is the band-pass-filtered 9-day perturbations in parallel electric field E_{PAR} on the respective days. As expected, the periodic oscillations in EEJ and WEJ are well in-phase with E_{PAR} oscillations, while the periodic oscillations in Lat-EEJ and Lat-WEJ are opposite phase with E_{PAR} oscillations. The opposite phase means that the electrojet central latitude shifts equatorward (poleward) as E_{PAR} increases (decreases). Additionally, the perturbations in these electrojet parameters exhibit significant MLT dependence.

5. Discussion

[11] The auroral electrojets are mostly Hall currents flowing in the east-west direction and controlled mainly by the north-south component of the electric field and the Hall conductance over the region. According to *Kamide and Kokubun* [1996] and *Ahn et al.* [1999, 2000], the eastward electrojet fluctuation is largely due to that of the electric field, while the westward electrojet fluctuation is attributed to both the electric field and Hall conductance. Moreover, there are two sources of ionospheric conductance: one is associated with the solar EUV radiation varying smoothly and maximizing near local noon and the other with auroral particle precipitation, which shows a maximum around local midnight [*Ahn et al.*, 1999]. These suggest that the variations of the auroral electrojets are actually controlled by two types of external energy sources, solar wind forcing (including directly driven processes and loading-unloading processes), and solar EUV irradiance. During the solar minimum in 2008, the EUV irradiance does not exhibit any significant spectral peaks at the period of 9 days [*Tulasi Ram et al.*, 2010]. Therefore the 9-day periodicity in the auroral

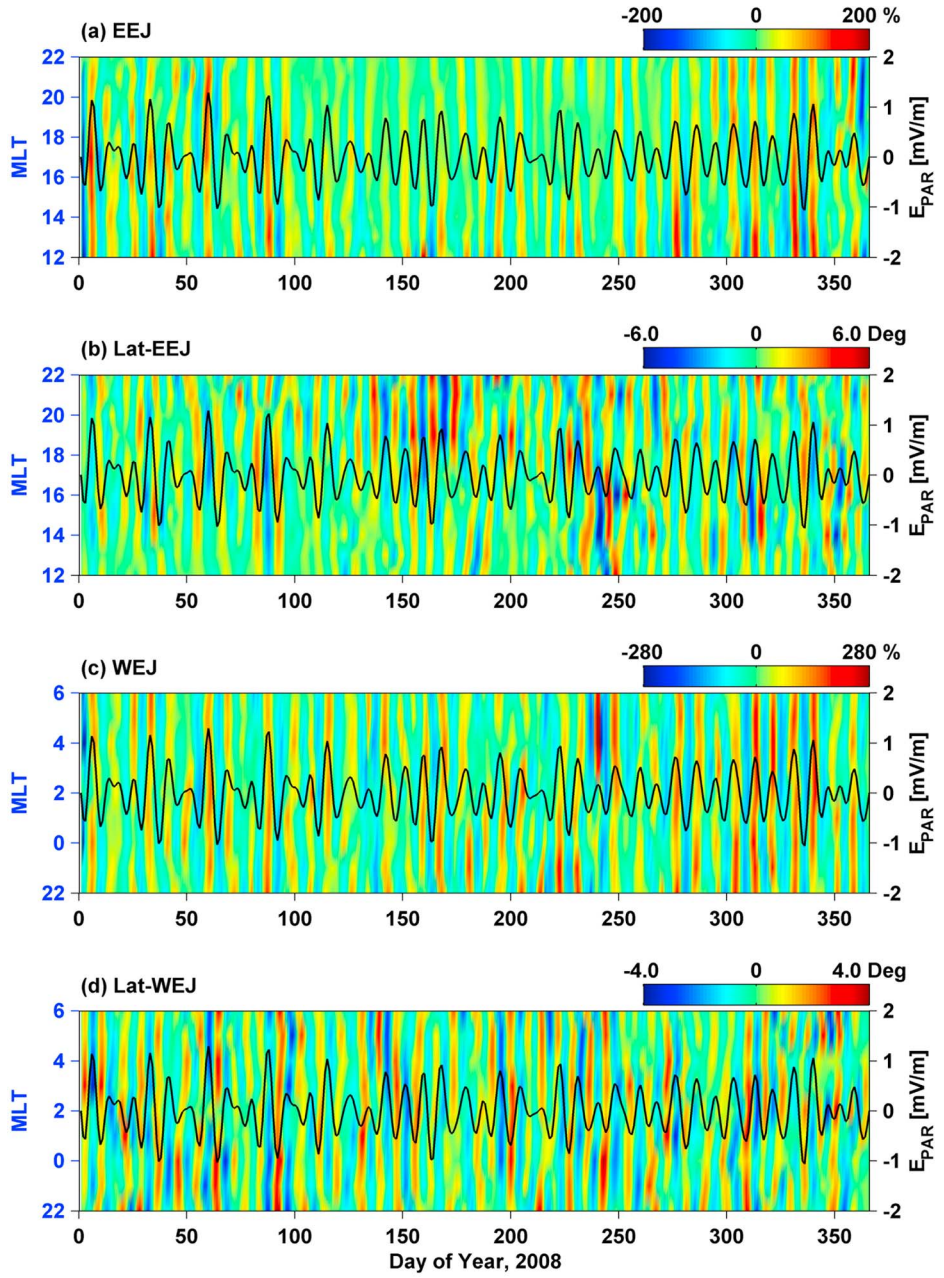

Figure 5. Band-pass filtered 9-day perturbations in (a) EEJ, (b) Lat-EEJ, (c) WEJ, and (d) Lat-WEJ as a function of MLT and day number. The 9-day perturbations in parallel electric field E_{PAR} are also overlapped as the black curve (right-hand scale). In order to better visualize the 9-day periodicity, the EEJ and WEJ perturbations are represented in percent perturbations relative to 11-day running means, whereas the Lat-EEJ and Lat-WEJ perturbations are shown in absolute numerical values. The band-pass filter is centered at the period of 9 days, with half-power points at 6 and 12 days.

electrojet activity is solely attributed to the recurrent solar wind forcing. In addition, the observed auroral electrojet response to the recurrent solar wind forcing offers several opportunities: (1) to estimate the contribution of the electric field to the eastward electrojet in the postnoon sector, (2) to isolate the Hall conductance associated with particle precipitation in the midnight-postmidnight sector, and (3) to gain new physical insight into the processes governing the eastward and westward auroral electrojets.

[12] In order to investigate the cause and effect relationship between recurrent HSSs and auroral electrojet activity, we proceed with a cross-correlation analysis. The band-pass-filtered 9 day periodic perturbations in electrojet parameters (EEJ, Lat-EEJ, WEJ, and Lat-WEJ) in each MLT bin are cross-correlated with the perturbations in solar wind parameters as well as particle precipitation during the entire year 2008, and the zero-lag correlation coefficients (r) are plotted in Figure 6. For the total currents, the correlation

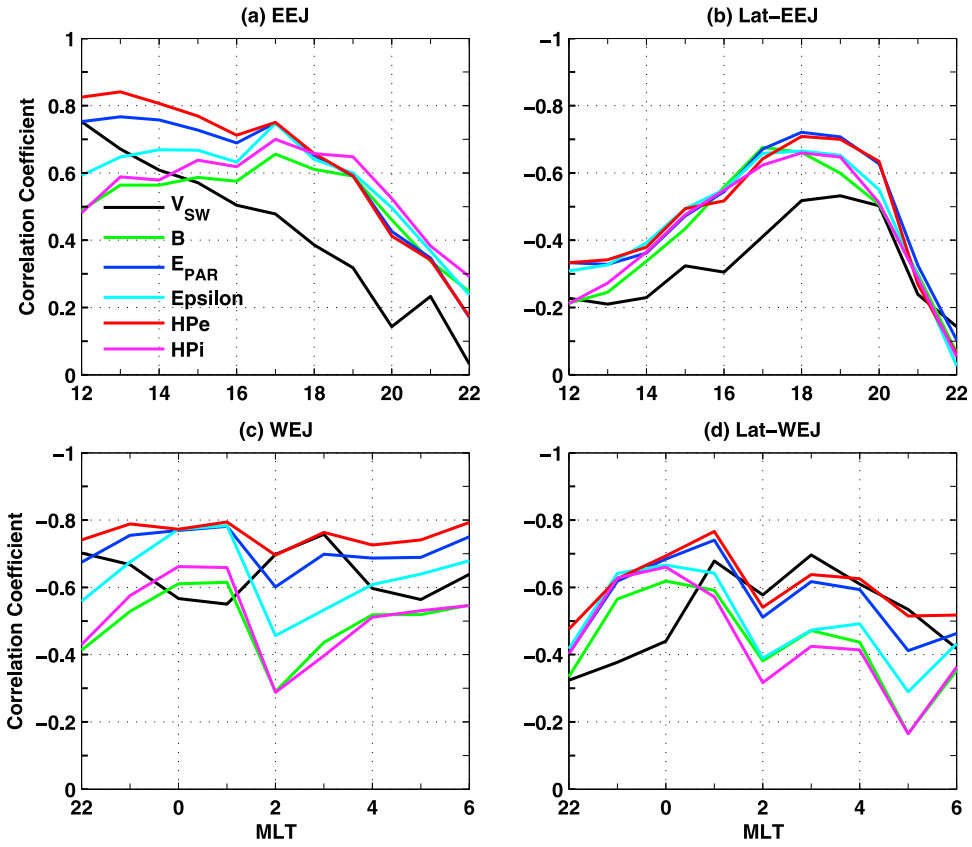

Figure 6. MLT variation of correlation coefficient (r) obtained from the zero-lag cross correlation of band-pass filtered 9-day perturbations in (a) EEJ, (b) Lat-EEJ, (c) WEJ, and (d) Lat-WEJ with the perturbations in various parameters (solar wind velocity V, interplanetary magnetic field B, parallel electric field E_{PAR}, epsilon parameter, HPe and HPi) during the entire year of 2008.

coefficients reveal two obvious features: (1) both the eastward and westward electrojet currents are better correlated with parallel electric field E_{PAR} and electron hemispheric power (HPe) than with other forcing parameters; (2) the eastward electrojet shows good correlations ($r > 0.6$) with E_{PAR} and HPe only in part of its optimal MLT sector, roughly 1200–1800, while the westward electrojet shows good correlations ($r < -0.6$) with E_{PAR} and HPe in its whole optimal MLT sector. Because there is no significant particle precipitation in local time sector 1200–1800 MLT [*Ahn et al.*, 1999], the correlation between the eastward electrojet and E_{PAR} is created by the cross-polar electric field coupled to the solar wind electric field [*Weimer*, 2005]. On the other hand, the westward electrojet correlation is associated with particle precipitation driven by magnetotail convection driven by the solar wind electric field [*Ahn et al.*, 1992]. Finally, the poor correlations in the MLT sector 1800–2200 might be attributed to the impact of other magnetosphere-ionosphere coupling processes associated with energy release in the magnetotail. As mentioned above, the 9-day perturbations in the westward electrojet carry the contributions from both the electric field and the Hall conductance, and the Hall conductance is caused solely by particle precipitation. Therefore the high correlation between 9-day perturbations in HPe and those in the westward electrojet is as expected. However, to understand the relative contribution of the electric field and the Hall conductance, additional data sources such as the electric field data and model simulations are required.

[13] Further, we investigate the sensitivities of the auroral electrojet variations to periodic solar wind forcing for the year 2008. The parallel electric field E_{PAR} is selected to represent the solar wind forcing, and this analysis focuses on the MLT regions where there is a good correlation ($|r| > 0.6$) between E_{PAR} and electrojet parameters (cf. Figure 6). Figure 7 shows the sensitivities of the 9-day perturbations in EEJ, Lat-EEJ, WEJ, and Lat-WEJ to those in E_{PAR}. As we can see, the auroral electrojet parameters tend to saturate when the E_{PAR} perturbations exceed -0.7 or 0.7 mV/m approximately. For the E_{PAR} perturbations between -0.7 and 0.7 mV/m, the black lines are the best linear fit, which show that the sensitivities of EEJ and Lat-EEJ to E_{PAR} are close to 0.06 MA/(mV/m) and -2.83 Deg/(mV/m), respectively, and the sensitivities of WEJ and Lat-WEJ to E_{PAR} are close to -0.12 MA/(mV/m) and -2.14 Deg/(mV/m), respectively. Note that the quantitative relationship between parallel electric field and total current also depends on the background level.

6. Concluding Remarks

[14] The IMAGE network magnetic measurements are used to study the response of the auroral electrojets to the

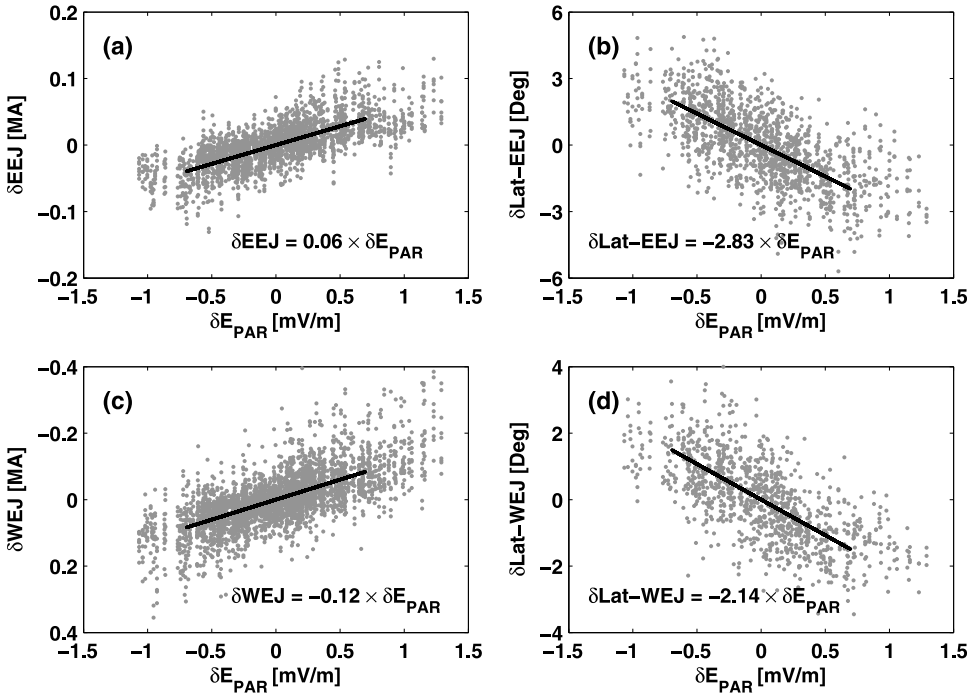

Figure 7. (a) Sensitivity of the 9-day perturbations in EEJ to those in E_{PAR} for the MLT regions where there is a good correlation ($|r| > 0.6$) between them. The linear fit is plotted out in the black line when the E_{PAR} perturbations lie between −0.7 and 0.7 mV/m. Same as Figure 7a except for sensitivity of (b) Lat-EEJ, (c) WEJ, and (d) Lat-WEJ to E_{PAR}, respectively.

recurrent high-speed solar wind streams (HSSs) during the extreme solar minimum period of 2008. The parameters examined consist of the total current of the eastward and westward electrojets, the central latitude of the electrojets, and the auroral eletrojet indices (IU and IL) created from the IMAGE magnetometer data in a manner similar to the global AU and AL indices. The main conclusions of this study are summarized as follows:

[15] 1. In MLT sectors 1230–2230 (for IU) and 2230–0630 (for IL), the strength of the limited UT sector index is on average larger than the simultaneous global index (AU/AL). This indicates that in these local times, the IU/IL indices are the better proxies for the global activity.

[16] 2. The 9-day periodicity found in the total eastward and westward electrojet currents and their central latitudes is consistent with a similar periodicity present in solar wind parameters as well as auroral particle precipitation, indicating a clear solar-terrestrial connection between auroral electrojet oscillations and recurrent HSSs rooted in rotating holes.

[17] 3. For the 9-day perturbations, both the eastward and westward electrojet currents are better correlated with parallel electric field (E_{PAR}) and electron hemispheric power (HPe) than with other forcing parameters. Interestingly, the eastward electrojet shows good correlations ($r > 0.6$) with E_{PAR} and HPe only in part of its optimal MLT sector, roughly 1200–1800, while the westward electrojet shows good correlations ($r < -0.6$) with E_{PAR} and HPe in its whole optimal MLT sector. The poor correlations between the eastward electrojet and E_{PAR} and HPe in the MLT sector 1800–2200 might be attributed to the impact of other magnetosphere-ionosphere coupling processes associated with energy release in the magnetotail.

[18] 4. The sensitivities of the eastward and westward electrojet currents to parallel electric field E_{PAR} are close to 0.06 MA/(mV/m) and −0.12 MA/(mV/m), respectively, and the sensitivities of their central latitudes to E_{PAR} are close to −2.83 Deg/(mV/m) and −2.14 Deg/(mV/m), respectively.

[19] **Acknowledgments.** This work is jointly supported by the National Natural Science Foundation of China (40921063, 40890162, 41031066, 40904049, 41004082, and 41174139), the 973 program (2012CB825601), the Specialized Research Fund for State Key Laboratories, and Ocean Public Welfare Scientific Research Project (201005017), State Oceanic Administration People's Republic of China. The work of ET was supported by Finnish Academy projects 108518, 128632, and 121289. The OMNI solar wind database is compiled by the Space Physics Data Facility at the Goddard Space Flight Center. The original DMSP and NOAA satellite auroral hemispheric power estimates were provided by the USAF Research Laboratory, Hanscom AFB, Massachusetts, and by the Space Weather Prediction Center, Boulder, Colorado, via the Coupling, Energetics and Dynamics of Atmospheric Regions (CEDAR) Database, which is supported by the National Science Foundation. NOAA electron hemispheric powers, which could infer ion hemispheric powers from the total, were supplied by David S. Evans of the Space Weather Prediction Center at the National Oceanic and Atmospheric Administration (NOAA). We thank the institutes who maintain the IMAGE Magnetometer Array.

[20] Robert Lysak thanks the reviewers for their assistance in evaluating this paper.

References

Ahn, B.-H., Y. Kamide, H. W. Kroehl, and D. J. Gorney (1992), Cross-polar cap potential difference, auroral electrojet indices, and solar wind parameters, *J. Geophys. Res.*, *97*(A2), 1345–1352, doi:10.1029/91JA02432.

Ahn, B.-H., B. Emery, H. Kroehl, and Y. Kamide (1999), Climatological characteristics of the auroral ionosphere in terms of electric field and

ionospheric conductance, *J. Geophys. Res.*, *104*(A5), 10,031–10,040, doi:10.1029/1999JA900043.

Ahn, B.-H., H. Kroehl, Y. Kamide, and E. Kihn (2000), Seasonal and solar cycle variations of the auroral electrojet indices, *J. Atmos. Sol. Terr. Phys.*, *62*, 1301–1310, doi:10.1016/S1364-6826(00)00073-0.

Akasofu, S.-I. (1981), Energy coupling between the solar wind and the magnetosphere, *Space Sci. Rev.*, *28*, 121–190, doi:10.1007/BF00218810.

Amm, O., and A. Viljanen (1999), Ionospheric disturbance magnetic field continuation from the ground to the ionosphere using spherical elementary current systems, *Earth Planets Space*, *51*, 431–440.

Emery, B. A., V. Coumans, D. S. Evans, G. A. Germany, M. S. Greer, E. Holeman, K. Kadinsky-Cade, R. J. Rich, and W. Xu (2008), Seasonal, Kp, solar wind, and solar flux variations in long-term single-pass satellite estimates of electron and ion auroral hemispheric power, *J. Geophys. Res.*, *113*, A06311, doi:10.1029/2007JA012866.

Emery, B. A., I. G. Richardson, D. S. Evans, R. J. Rich, and W. Xu (2009), Solar wind structure sources and periodicities of global electron hemispheric power over three solar cycles, *J. Atmos. Sol. Terr. Phys.*, *71*, 1157–1175, doi:10.1016/j.jastp.2008.08.005.

Gibson, S. E., J. U. Kozyra, G. de Toma, B. A. Emery, T. Onsager, and B. J. Thompson (2009), If the Sun is so quiet, why is the Earth ringing? A comparison of two solar minimum intervals, *J. Geophys. Res.*, *114*, A09105, doi:10.1029/2009JA014342.

Kallio, E. I., T. I. Pulkkinen, H. E. J. Koskinen, A. Viljanen, J. A. Slavin, and K. Ogilvie (2000), Loading-unloading processes in the nightside ionosphere, *Geophys. Res. Lett.*, *27*(11), 1627–1630, doi:10.1029/1999GL003694.

Kamide, Y., and S. Kokubun (1996), Two-component auroral electrojet: Importance for substorm studies, *J. Geophys. Res.*, *101*(A6), 13,027–13,046, doi:10.1029/96JA00142.

Kauristie, K., T. I. Pulkkinen, R. J. Pellinen, and H. J. Opgenoorth (1996), What can we tell about the AE-index from a single meridional magnetometer chain?, *Ann. Geophys.*, *14*, 1177–1185.

Lei, J., J. Thayer, W. Wang, and R. McPherron (2011), Impact of CIR storms on thermosphere density variability during the solar minimum of 2008, *Sol. Phys.*, *274*, 427–437, doi:10.1007/s11207-010-9563-y.

Lomb, N. R. (1976), Least-squares frequency analysis of unequally spaced data, *Astrophys. Space Sci.*, *39*, 447–462, doi:10.1007/BF00648343.

Pulkkinen, A., et al. (2003), Ionospheric equivalent current distributions determined with the method of spherical elementary current systems, *J. Geophys. Res.*, *108*(A2), 1053, doi:10.1029/2001JA005085.

Pulkkinen, T. I., M. Palmroth, H. E. J. Koskinen, T. V. Laitinen, C. C. Goodrich, V. G. Merkin, and J. G. Lyon (2010), Magnetospheric modes and solar wind energy coupling efficiency, *J. Geophys. Res.*, *115*, A03207, doi:10.1029/2009JA014737.

Pulkkinen, T. I., E. I. Tanskanen, A. Viljanen, N. Partamies, and K. Kauristie (2011), Auroral electrojets during deep solar minimum at the end of solar cycle 23, *J. Geophys. Res.*, *116*, A04207, doi:10.1029/2010JA016098.

Scargle, J. D. (1982), Studies in astronomical time series analysis. Part II. Statistical aspects of spectral analysis of unevenly spaced data, *Astrophys. J.*, *263*, 835–853, doi:10.1086/160554.

Tanskanen, E. I. (2009), A comprehensive high-throughput analysis of substorms observed by IMAGE magnetometer network: Years 1993–2003 examined, *J. Geophys. Res.*, *114*, A05204, doi:10.1029/2008JA013682.

Tanskanen, E. I., T. I. Pulkkinen, and H. E. J. Koskinen (2002), Substorm energy budget near solar minimum and maximum: 1997 and 1999 compared, *J. Geophys. Res.*, *107*(A6), 1086, doi:10.1029/2001JA900153.

Tanskanen, E. I., J. A. Slavin, A. J. Tanskanen, A. Viljanen, T. I. Pulkkinen, H. E. J. Koskinen, A. Pulkkinen, and J. Eastwood (2005), Magnetospheric substorms are strongly modulated by interplanetary high-speed streams, *Geophys. Res. Lett.*, *32*, L16104, doi:10.1029/2005GL023318.

Tsurutani, B. T., W. D. Gonzalez, A. L. C. Gonzalez, F. Tang, J. K. Arballo, and M. Okada (1995), Interplanetary origin of geomagnetic activity in the declining phase of the solar cycle, *J. Geophys. Res.*, *100*(A11), 21,717–21,733, doi:10.1029/95JA01476.

Tulasi Ram, S., C. H. Liu, and S.-Y. Su (2010), Periodic solar wind forcing due to recurrent coronal holes during 1996–2009 and its impact on Earth's geomagnetic and ionospheric properties during the extreme solar minimum, *J. Geophys. Res.*, *115*, A12340, doi:10.1029/2010JA015800.

Weimer, D. R. (2005), Improved ionospheric electrodynamic models and application to calculating Joule heating rates, *J. Geophys. Res.*, *110*, A05306, doi:10.1029/2004JA010884.

B. A. Emery, High Altitude Observatory, National Center for Atmospheric Research, 3080 Center Green, Boulder, CO 80301, USA. (emery@ucar.edu)

X. Feng and J. Guo, SIGMA Weather Group, State Key Laboratory of Space Weather, Center for Space Science and Applied Research, Chinese Academy of Sciences, 1 Nanertiao, Zhongguancun, Haidian District, Beijing 100190, China. (jpguo@spaceweather.ac.cn; fengx@spaceweather.ac.cn)

J. Lei, School of Earth and Space Sciences, University of Science and Technology of China, Hefei, Anhui 230026, China. (leijh@ustc.edu.cn)

T. I. Pulkkinen, School of Electrical Engineering, Aalto University, PO Box 13000, FI-00076 Aalto, Finland. (tuija.i.pulkkinen@aalto.fi)

E. I. Tanskanen, Finnish Meteorological Institute, PO Box 503, FI-00101 Helsinki, Finland. (eija.tanskanen@fmi.fi)

W. Xu, Institute of Geology and Geophysics, Chinese Academy of Sciences, 19 Beitucheng Western Rd., Beijing 100029, China. (wyxu@mail.iggcas.ac.cn)